Applied Numerical Modeling in Geomechanics – 2020 – Billaux, Hazzard, Nelson & Schöpfer (eds.) Paper: 05-02

Dynamic analysis of fault-slip velocity in longwall mining

Chunchen Wei, Chengguo Zhang & Ismet Canbulat
School of Minerals and Energy Resources Engineering, University of New South Wales, Sydney NSW 2052, Australia

1 INTRODUCTION

Coal burst has been a major problem in underground mining for decades (Mark 2016). There are many factors that can result in coal burst, such as deep cover depth, massive rock layers above or below the coal seam, faults and other geological problems (Ortlepp 2005, Iannacchione & Tadolini 2016, Zhang et al. 2017). Of these causal factors, Ortlepp (2005) stated that fault slip is a significant factor that can produce higher potential seismic energy than the other factors. The seismic wave generated by fault slip is able to propagate to the excavations around the fault. Coal mass around the excavations will then experience not only static loading but also dynamic loading produced by the seismic wave. Coal burst is highly likely to occur if the combined static loading and dynamic loading is high enough (Dou et al. 2014). The risk is even higher when the excavation is close to the major fault (Cai et al. 2014, Sainoki & Mitri 2014).

This paper analyses the source mechanisms of fault-slip behavior using a *FLAC3D* (Itasca 2017) numerical model, in which a longwall face approached a major reverse fault with 70° of fault angle. The Mohr-Coulomb strain softening constitutive model was applied to the rock mass in longwall model. The fault was simulated by the build in zero-thickness interface elements. The post failure process of fault-slip was studied using the linear slip weakening law which was implemented in a user-defined *FISH* program. The static numerical analysis was conducted at the beginning of longwall excavations. Once the fault began to slip, the dynamic numerical analysis was carried out to study the dynamic fault-slip behavior. The fault-slip velocity and the dynamic impact of seismic waves are analyzed in this study.

2 DESIGN AND ANALYSIS

A series of global models were established using *FLAC3D*. As seen in Figure 1, the models are 2D in nature (y-direction is 1 m of thickness). The green line represents a major fault and the layer in black is the coal seam. There are 7 rock layers in the z-direction. The thickness of each layer is shown in Table 1. For height in the model, the top boundary is 150 m above the coal seam and the bottom boundary is 90 m below the coal seam. The longwall face was extracted from the starting line all the way to the fault and finally crossed the fault to stop at the end line. For model length, the starting line is 100 m to the right boundary and 480 m to the end line. The distance between the left boundary and the end line is 140 m.

The linear slip weakening law is given by Eq. 1, which was implemented to simulate the post failure process of fault-slip during longwall excavations.

$$\tau = \tau_s - (\tau_s - \tau_d)\frac{u}{D_C}, (u \le D_C)$$
$$\tau = \tau_d \quad (1)$$

Where τ is the shear strength of the fault, τ_s is the static shear strength, τ_d is the dynamic shear strength, u is the slip distance, D_C is the critical slip distance.

For excavations, the coal seam and immediate roof were extracted together. The thickness of the immediate roof was four times the coal seam thickness. The abutment angle was kept constant at 20°. For the first 380 m, the excavation length was 10 m per step. It then decreased to 5 m per excavation step when the longwall face was within 100 m to the end line. Elastic goaf material with 500 MPa of Young's modulus was used to fill in the goaf area during extractions.

For static boundary conditions, a vertical load determined by cover depth was put on the top boundary. The horizontal boundaries were fixed only in their normal direction. The bottom boundary was fixed in all directions. The initial horizontal stress applied in the model is given by (Esterhuizen et al. 2010), as shown in Equation 2:

$$\sigma_{\mathrm{h\,max}} = 1.2\sigma_v + 2.6 + 0.003E$$
$$\sigma_{\mathrm{h\,min}} = 1.2\sigma_v + 0.0015E \quad (2)$$

Where E is the elastic modulus of each rock layer and σ_v is the vertical overburden stress, σ_{hmax} is the maximum horizontal principal stress (in x-direction) and σ_{hmin} is the minimum horizontal principal stress (in y-direction).

The mechanical properties of the rock layers and the coal seam are summarized in Table 1. A strain softening failure criterion was applied to all rock layers. Residual tension was set at 0 MPa and residual cohesion was set to 10% of the peak cohesion for all rock layers. The mechanical properties of rock layers were obtained from Zipf (2006), as seen in Table 1, in which the parameters are designed for coal mining simulation in *FLAC3D*. The field UCS and model parameters in this table are reduced from the laboratory-scale values obtained from point load tests during geologic logging. The reduction factor is 0.56 which is recommended by Gale and Tarrant (1997). Following the recommendation of Zipf (2006) again, as shown in Table 1, the residual tension was set to 0 MPa and the residual cohesion was set to 10% of the peak cohesion for all rock layers in Table 1. The values of tension and cohesion decreased from the peak value to the residual value were over 1% and 5% of plastic strain, respectively.

Table 1. Mechanical properties used for rock layers.

Material	Thickness /m	E (Young's) /GPa	Poisson	Cohesion /MPa	Friction /°	Tension /MPa
Shale	111	6	0.25	4.5	25	1.4
Sandstone	18	8	0.25	8	28	2.7
Shale	6	6	0.25	4.5	25	1.4
Shale	12	5	0.25	3.3	24	1.0
Coal seam	3	3	0.25	1.2	28	1
Shale	20	6	0.25	4.5	25	1.4
Shale	70	7	0.25	6	26	1.9

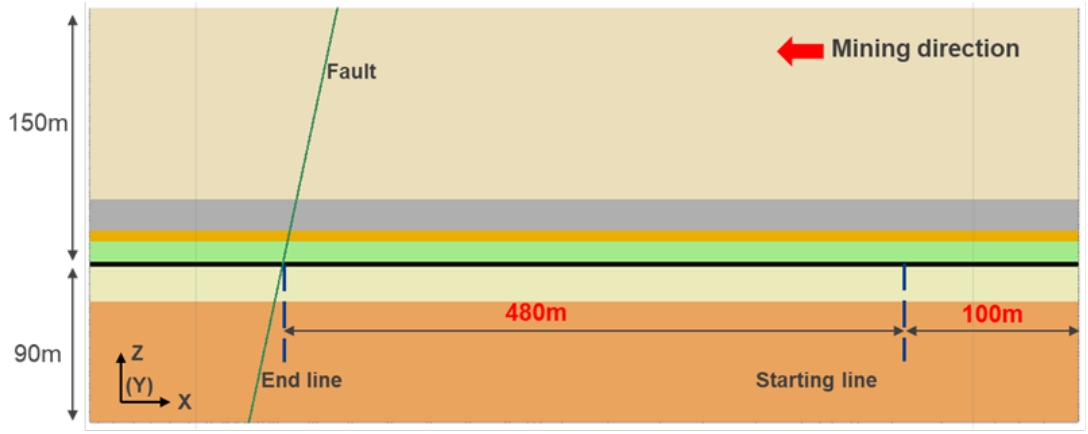

Figure 1. Schematic diagram of the basic models.

For dynamic analysis, the boundary conditions were changed to viscous in order to prevent the model boundaries from reflecting elastic waves arising from fault slip and the extraction of longwall panel. The timestep used for the dynamic analysis is automatically calculated based on the volume of each zone of the model, P-wave velocity obtained from rock mass mechanical properties and the face area of each zone (Itasca 2006). This study takes 5% of critical damping in the dynamic analysis.

3 RESULTS AND CONCLUSIONS

In static analysis, the results showed that the fault began to slip when the longwall face was 50 m away from the fault. The fault-slip area appeared first at approximately 39 m above the coal seam, as shown in Figure 2.

Next, the dynamic analysis was conducted. A monitoring point was set up close to the initiation fault-slip area (shown in Fig. 2). The maximum slip velocity at this area was approximately 0.04 m during the dynamic analysis as shown in Figure 3.

Other than that, the slip velocity of the interface nodes was monitored using a user-defined *FISH* program. The fault-slip process can be clearly shown in Figure 4. At 0.08s, the slip velocity reached to 0.028 m/s at approximately 40 m above the coal seam. Then the fault-slip front moved upwards along the fault and the slip velocity reached to 0.04 m/s at 0.16 s.

Figure 5 shows the dynamic fault-slip process since the fault started to slip. It shows clearly that the seismic wave with butterfly-pattern was produced by the fault-slip. The seismic wave gradually propagated to the longwall excavation and generated dynamic impact on the excavation boundaries.

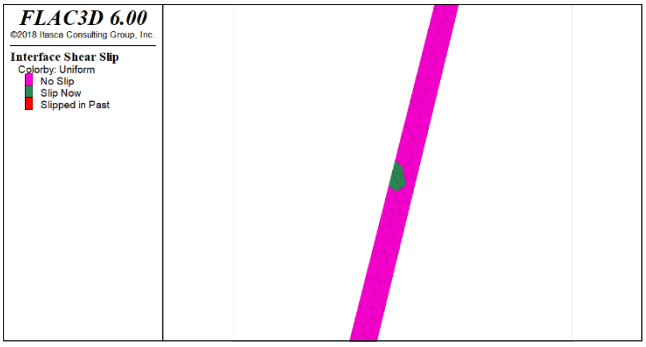

Figure 2. Fault-slip initiation.

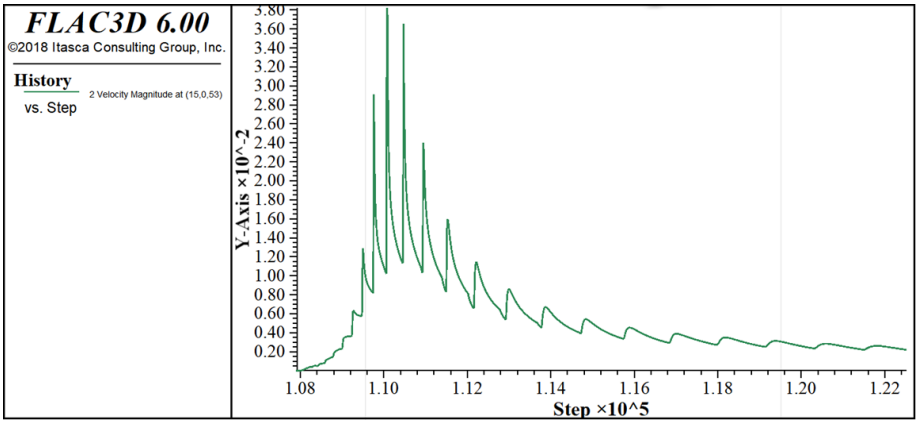

Figure 3. Zone velocity close to the fault.

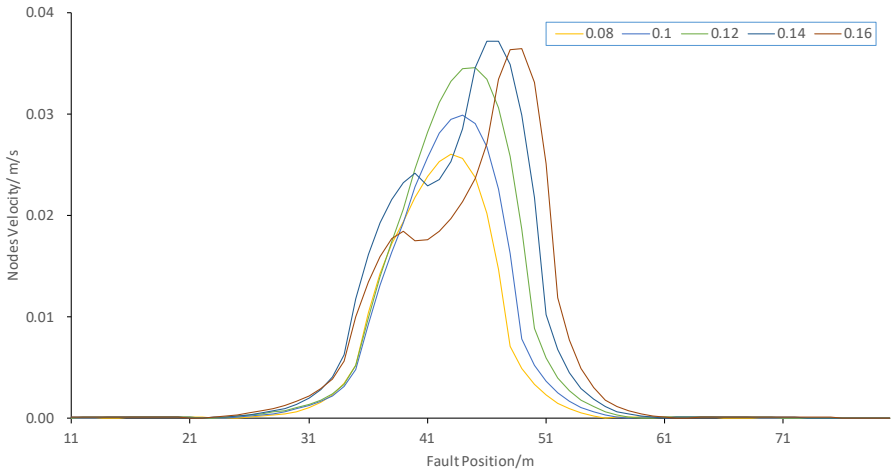

Figure 4. Slip process along the fault.

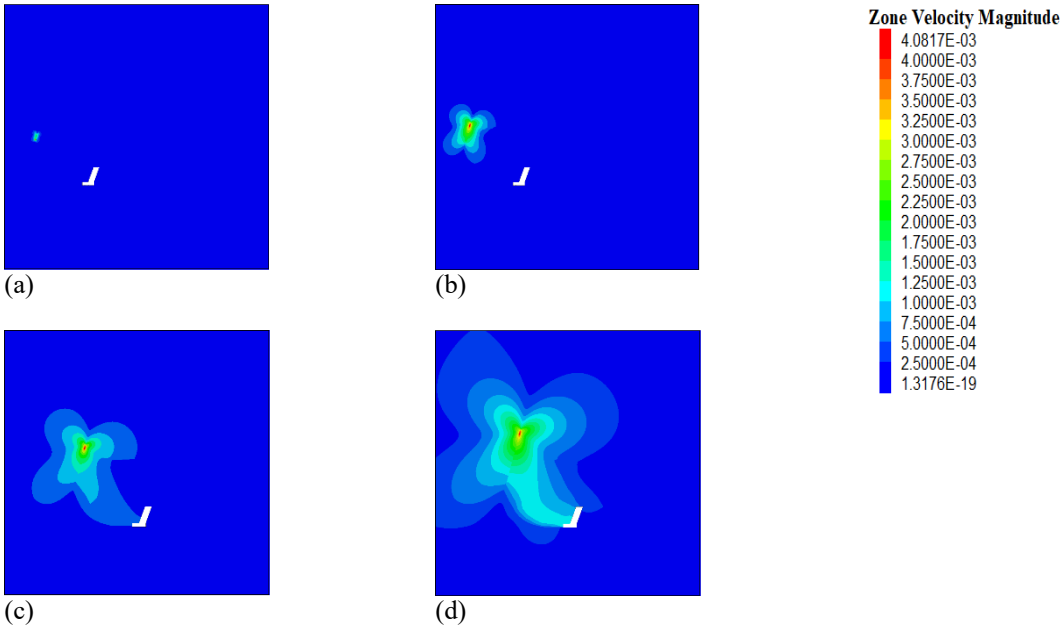

Figure 5. Seismic wave produced by fault-slip in dynamic analysis.

REFERENCES

Cai, W., Dou, L., Cao, A., Gong, S. & Li, Z. 2014. Application of seismic velocity tomography in underground coal mines: a case study of Yima mining area, Henan, China, *Journal of Applied Geophysics,* 109, 140-149.

Dou, L., Mou, Z., Li, Z., Cao, A. & Gong, S. 2014. Research progress of monitoring, forecasting, and prevention of rockburst in underground coal mining in China, *International Journal of Coal Science & Technology,* 1(3), 278-288.

Esterhuizen, E., Mark, C. & Murphy, M.M. 2010. Numerical model calibration for simulating coal pillars, gob and overburden response, in *Proceedings of the 29th International Conference on Ground Control in Mining, Morgantown, WV*, pp 46-57.

Gale, W. & Tarrant, G. 1997. Let the rocks tell us, in *Proceedings of the Symposium on Safety in Mines: The Role of Geology*, pp 153-160.

Iannacchione, A. & Tadolini, S.C. 2016. Occurrence, prediction, and control of coal burst events in the US, *International Journal of Mining Science and Technology,* 26(1), 39-46.

Itasca Consulting Group, Inc., 2006. *FLAC3D - Fast Lagrangian Analysis of Continua in 3 Dimensions, Ver. 3.1, User's Manual*. Minneapolis: Itasca.

Itasca Consulting Group, Inc., 2017. *FLAC3D - Fast Lagrangian Analysis of Continua in 3 Dimensions, Ver. 6.0,* Minneapolis: Itasca.

Mark, C. 2016. Coal bursts in the deep longwall mines of the United States, *International Journal of Coal Science & Technology,* 3(1), 1-9.

Ortlepp, W. 2005. RaSiM comes of age—a review of the contribution to the understanding and control of mine rock-bursts, in *Proceedings of the Sixth International Symposium on Rockburst and Seismicity in Mines, Perth, Western Australia*, pp 9-11.

Sainoki, A. & Mitri, H.S. 2014. Dynamic modelling of fault-slip with Barton′ s shear strength model, *International Journal of Rock Mechanics and Mining Sciences,* 67, 155-163.

Zhang, C., Canbulat, I., Hebblewhite, B. & Ward, C.R. 2017. Assessing coal burst phenomena in mining and insights into directions for future research, *International Journal of Coal Geology,* 179, 28-44.

Zipf, K. 2006. Numerical modeling procedures for practical coal mine design, in *Proceedings Golden Rocks 2006, The 41st US Symposium on Rock Mechanics (USRMS)* (American Rock Mechanics Association).